IEEE Access
Multidisciplinary ⋮ Rapid Review ⋮ Open Access Journal

Received 30 September 2023, accepted 16 October 2023, date of publication 20 October 2023, date of current version 31 October 2023.

Digital Object Identifier 10.1109/ACCESS.2023.3326415

RESEARCH ARTICLE

Enhancing Power Generation Forecasting in Smart Grids Using Hybrid Autoencoder Long Short-Term Memory Machine Learning Model

AHSAN ZAFAR[1], YANBO CHE[1], (Member, IEEE), MUNEER AHMED[1], MUHAMMAD SARFRAZ[2], ASHFAQ AHMAD[3], AND MOHAMMAD ALIBAKHSHIKENARI[4], (Member, IEEE)

[1]Key Laboratory of Smart Grid of Ministry of Education, School of Electrical and Information Engineering, Tianjin University, Tianjin 300072, China
[2]School of Electrical and Information Engineering, Tianjin University, Tianjin 300072, China
[3]Department of Chemistry, College of Science, King Saud University, Riyadh 11451, Saudi Arabia
[4]Department of Signal Theory and Communications, Universidad Carlos III de Madrid, Leganés, 28911 Madrid, Spain

Corresponding authors: Yanbo Che (ybche@tju.edu.cn) and Mohammad Alibakhshikenari (mohammad.alibakhshikenari@uc3m.es)

Dr. Mohammad Alibakhshikenari acknowledges support from the CONEX-Plus programme funded by Universidad Carlos III de Madrid and the European Union's Horizon 2020 research and innovation programme under the Marie Sklodowska-Curie grant agreement No. 801538. Additionally, Dr. Ashfaq Ahmad sincerely appreciates funding from Researchers Supporting Project number (RSPD2023R666), King Saud University, Riyadh, Saudi Arabia.

ABSTRACT This study explores the implementation of advanced machine learning techniques to enhance the integration of renewable energy into smart grids, focusing specifically on predicting solar power generation for the upcoming year. Three distinct machine learning models are employed: the Long Short-Term Memory (LSTM), Bidirectional Long Short-Term Memory (Bi-LSTM) and a hybrid model that combines Autoencoder and Long Short-Term Memory (AE-LSTM). Using real-time solar power production data spanning a year, these models are trained and evaluated using mean absolute error (MAE) and mean squared error (MSE) as performance metrics. Results highlight the superior accuracy of the hybrid AE-LSTM model compared to the LSTM model as well as Bi-LSTM model, attributed to its capability to capture intricate temporal patterns and correlations within the data. This research underscores the significant potential of machine learning techniques, particularly the hybrid AE-LSTM approach, in facilitating the seamless integration of renewable energy resources into smart grids, contributing to more efficient and environmentally conscious power systems. Furthermore, a comprehensive analysis reveals the hybrid AE-LSTM model's capacity to produce superior predictions due to its additional training, solidifying its advantage over models solely reliant on the other model's architecture. In summary, this study demonstrates the effectiveness of advanced machine learning methodologies in revolutionizing renewable energy integration, with the hybrid AE-LSTM model standing out as a promising avenue for enhanced prediction accuracy.

INDEX TERMS Renewable energy, smart grids, power forecasting, bi-LSTM model, hybrid autoencoder LSTM model.

I. INTRODUCTION

As global concerns increasingly center around long-term sustainability, the imperative for environmentally sound and sustainable energy sources has grown more pronounced. The dwindling availability of non-renewable resources like fossil fuels not only threatens resource scarcity but also poses severe environmental risks. Consequently, alternative renewable energy sources, such as solar, wind, and hydroelectricity, have been gaining substantial traction [1]. Yet, the integration of these renewable assets into intelligent electricity grids presents multifaceted challenges. Scholars are responding by

The associate editor coordinating the review of this manuscript and approving it for publication was Long Xu.

innovating hybrid solutions aimed at bolstering grid stability and refining control mechanisms [2], [3], [4], [5]. These inventive approaches encompass specific control methodologies to enhance failure ride-through capabilities, voltage regulation, and reactive power injection, effectively addressing the complexities of grid failures. This endeavor draws support from meticulous comparative analyses and simulation findings, which further chart a course for prospective research directions [2], [3], [4], [5]. Looking ahead, the role of artificial intelligence (AI) techniques in smart grid management, spanning wind, solar, and biogas systems, is poised for pivotal significance [6], [7]. An illustrative breakthrough lies in a groundbreaking system designed by researchers for tracking solar panels within photovoltaic power stations. This novel system harnesses algorithms and image-processing methodologies, underscoring the growing reliance on technologies like UAVs and automated recognition [8], [9]. Solar energy's ascendancy in meeting energy demands is evident [10]. However, accurate prediction of solar plant energy output remains a formidable challenge, necessitating advanced methodologies [11]. The limitations of conventional forecasting approaches, especially in predicting power generation and related attributes, have spurred researchers to explore diverse models, particularly those rooted in machine learning. The utilization of data from diverse energy and electricity sources has underscored the significant predictive capabilities of these models [12]. Illustratively, hybrid models that amalgamate ARIMA and LSTM techniques have shown promise in short-term electric energy forecasts for photovoltaic power plants. By capitalizing on the strengths of both approaches, these models strive to elevate the accuracy of power supply forecasts [13], [14]. Similarly, Bi-LSTM models have been exclusively applied to anticipate energy parameter production within solar plants. These models consider temporal and spatial interdependencies to refine the accuracy of predictions [15], [16]. Nevertheless, some studies exhibit a narrower focus on specific input features, potentially overlooking influential elements impacting electricity production [17]. The application of machine learning models extends beyond solar energy to include wind power prediction. Research investigating the effectiveness of ARIMA, LSTM, and ELM models in short-term wind power forecasting has revealed the superior accuracy of the ELM technique [18], [19]. Yet, certain studies in this domain fall short in clarifying model training and preprocessing procedures, which could compromise result reproducibility [20], [21], [22], [23]. While promising, machine learning models for energy forecasting are not devoid of limitations, including complexity, future data dependency, fixed-length input sequences, challenges in handling long-term dependencies, and the specter of overfitting. Researchers have explored alternative machine learning methodologies, exemplified by hybrid encoder-decoder designs that exhibit exceptional accuracy in predicting dynamic energy patterns in thermal power plants [24], [25]. In parallel, LSTM Auto-encoder models have demonstrated efficacy in forecasting solar plant production a day in advance, adeptly addressing data uncertainties and distortions [26], [27]. These models tap into deep learning frameworks like deep belief networks (DBN), LSTM neural networks, Autoencoders, and LSTM-recurrent neural networks (RNN) to estimate Photovoltaic production [28], [29], [30], [31]. Against this backdrop, the study's focus shifts towards assessing the efficacy of the Autoencoder LSTM (AE-LSTM) model in energy forecasting applications. Envisioned as a means to enhance the precision of time series predictions, this inquiry strives to conceive a hybrid model by fusing the Autoencoder with the Long Short-Term Memory (AE-LSTM) framework. The crux of this innovation lies in the Autoencoder LSTM's dual role—encoding sequential data while encapsulating temporal correlations. The preprocessing phase will meticulously tailor time series data to optimize input sequences, followed by comprehensive training and validation, leveraging methodologies like cross-validation.

This study's trajectory orbits around forecasting three pivotal metrics grounded in real-time solar plant data spanning a year: ''daily power generation,'' ''maximum grid-connected power generation,'' and ''radiance.'' It commences with the prediction of these parameters utilizing machine learning LSTM and Bi-LSTM models, followed by iterative refinement through the incorporation of the hybrid AE-LSTM approach. The crescendo of this effort will culminate in an intricate and holistic comparison of outcomes from both models, thereby facilitating a nuanced and comprehensive evaluation. Accordingly, the study is meticulously structured to delve into the design and methodology of the proposed models, their inherent differences, the context-specific case scenario, the intricacies of the dataset, the profound findings encompassing losses and forecasts, the intricacies of the employed system and software, and finally, encapsulating overarching insights gleaned from the research endeavor. The main contributions of this study are as follows:

- The key finding is that the hybrid AE-LSTM model demonstrates superior accuracy and performance compared to the other two benchmark models LSTM and Bi-LSTM model in predicting solar power generation for various parameters. The hybrid AE-LSTM model introduces a novel architecture that combines the feature extraction functionality of Autoencoders with the memory capabilities of LSTM networks.
- The study employs performance metrics such as MAE, MSE and RMSE to evaluate the effectiveness of the models. Results demonstrate that the hybrid AE-LSTM model consistently outperforms the LSTM as well as Bi-LSTM model across multiple parameters including ''daily power generation,'' ''maximum grid-connected power generation,'' and ''radiance.''
- By improving the accuracy of solar power generation predictions by hybrid AE-LSTM model. This contribution is crucial for enhancing decision-making processes

related to solar power facilities and optimizing resource distribution.
- The research underscores the potential AE-LSTM approach, in enhancing the integration of renewable energy resources into smart grids. This contribution aligns with the broader goal of developing more efficient and environmentally friendly power systems.

The paper is organized as follows: Section II outlines the design and methodology of the proposed models. This section not only explains the functioning of the models but also highlights the initial distinctions between the two. Moving on, Section III delves into the particulars of the specific case scenario and provides a comprehensive overview of the dataset. In Section IV, we thoroughly examine the findings of the study, encompassing both losses and forecasts. The technological infrastructure, including the system and software used to derive the experimental results, is elaborated upon in Section V. Finally, in Section VI, concluding insights drawn from the research are presented.

II. PROPOSED FRAMEWORK/METHODOLOGY

In the context of a stationary time-series dataset, this research employs a strategic approach utilizing three machine learning models: LSTM (Long Short-Term Memory), Bi-LSTM (Bidirectional Long Short-Term Memory) and a hybrid AE-LSTM (Autoencoder Long Short-Term Memory). The dataset comprises a year's worth of readings for three key parameters: ''daily power generation (kWh)'', ''maximum grid-connected power generation (MW)'', and ''radiance (MJ·m−2)''. These real-time measurements are sourced from a substantial solar power facility. To ensure a seamless time sequence, the dataset undergoes preprocessing to meet uninterrupted criteria. Initially, 80% of data is used as a training data while the remaining 20% data is used for the testing or validation.

For the testing set, the models' efficacy is evaluated, and adjustments are made to enhance accuracy. Validation data is then utilized to assess the models' performance with unseen data. With refined and validated models, the research extrapolates power generation for the subsequent year. This prediction involves extending the time series data into the future and predicting forthcoming values. The LSTM, Bi-LSTM and hybrid AE-LSTM models are leveraged for these power generation forecasts. These predictions offer actionable insights to solar power plant operators for resource allocation, pricing strategies, efficient power system planning, system stability, and key design considerations. The research outcomes prominently demonstrate that the hybrid Autoencoder LSTM model enhances accuracy and diminishes both mean absolute error (MAE) and mean squared error (MSE) compared to other two model. A comprehensive comparison of these models is thoughtfully incorporated within the study article. Furthermore, Fig. 1 visually delineates the comprehensive procedural flowchart along with visual outcomes derived from both models. In-depth elucidations of the structural and mathematical nuances of the LSTM, Bi-LSTM and AE-LSTM models are exhaustively covered in subsequent subsections.

A. STRUCTURE OF LSTM

An essential component of recurrent neural networks (RNNs), the Long Short-Term Memory (LSTM) cell, is designed to manage and capture dependencies within sequential data effectively. It accomplishes this through a well-structured composition of interconnected elements that enable the cell to selectively retain or forget information over time. The core structure of a simple LSTM cell as shown in Fig.2 comprises three crucial components: the input gate, the forget gate, and the output gate. These gates play pivotal roles in controlling the flow of information through the cell, while a memory cell continuously updates and stores data. In a Long Short-Term Memory (LSTM) neural network, there are four crucial gates that govern the flow of information. The input gate plays a pivotal role by assessing the importance of new data through a sigmoid activation function, considering both the current input and the previous hidden state. It selects essential elements from the input for storage in the memory cell. Conversely, the forget gate determines which data should be discarded from the memory cell, again considering the current input and the previous hidden state with a sigmoid activation function. The memory cell itself acts as a repository for persistent information, receiving input from the input gate to incorporate fresh data and from the forget gate to regulate information removal. Finally, the output gate decides how much information from the memory cell should be passed on to the next hidden state. It employs sigmoid activation to make this determination and further scales the output with a *tan* h activation function, constraining it within the range of −1 and 1. Together, these gates enable an LSTM to effectively manage and utilize information for various tasks in neural network processing. Collectively, these components empower the LSTM cell to make informed decisions about updating its memory, retaining crucial information, discarding irrelevant data, and generating outputs. With its unique architecture featuring a dedicated memory cell and gate-controlled information flow, LSTMs excel at capturing and preserving long-term relationships within sequential data.

B. MATHEMATICAL EXPRESSION OF LSTM

Within the architecture of the Long Short-Term Memory (LSTM) cell, there are three crucial gates: the forget gate, input gate, and output gate. These gates have the essential responsibility of governing the information flow inside the LSTM cell. Let's delve into a detailed explanation of the equations:

The forget gate assumes a pivotal role in determining which information should be retained or discarded from the previous time step's hidden state (h_{t-1}) and the current input (x_t). Its calculation involves the application of the sigmoid function (σ) to the weighted sum of inputs (W_f), as described

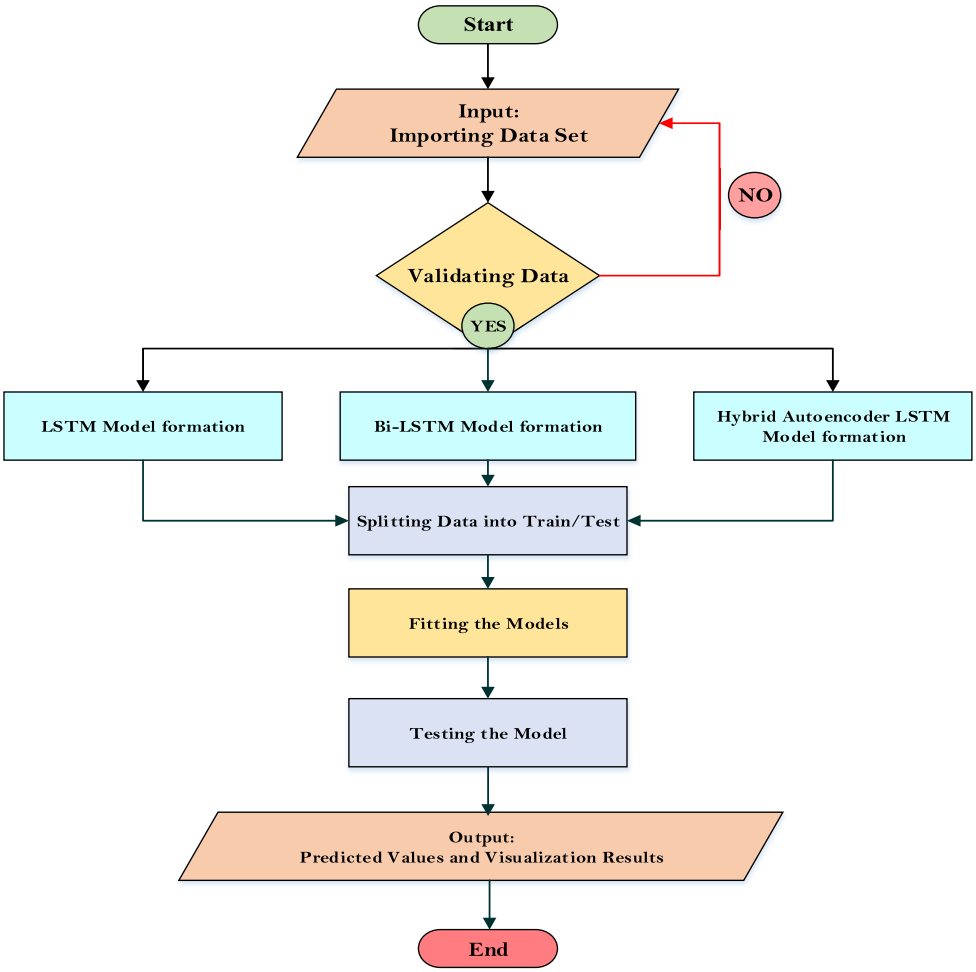

FIGURE 1. Results visualization process using LSTM, Bi-LSTM and AE-LSTM.

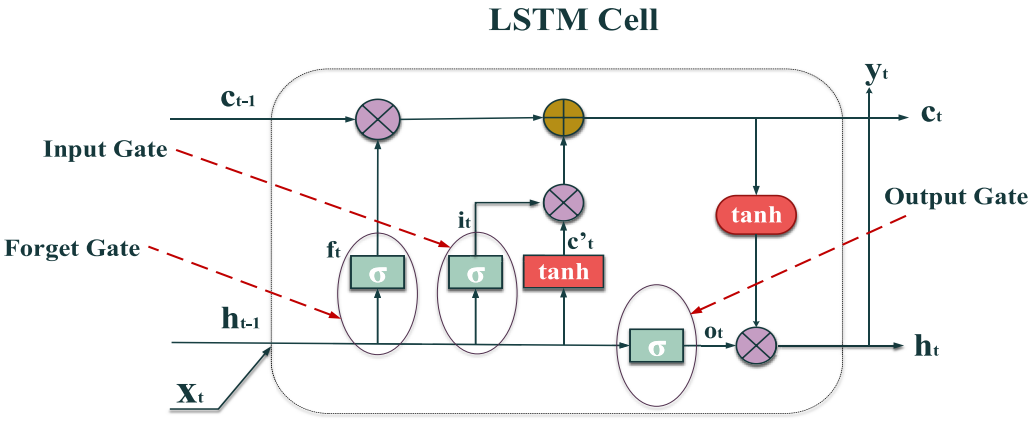

FIGURE 2. LSTM internal structure.

in Eq. (1):

$$f_t = \sigma\{W_f(h_{t-1}, x_t)\} \tag{1}$$

where σ represents the sigmoid function, W_f denotes the weighted sum of inputs within the forget gate, h_{t-1} represents the previous time step's hidden state, and x_t stands for the current input. The input gate determines which elements should be incorporated into the current cell state (f_t). It comprises two key components: first, an input gate layer employing the sigmoid function to select values for updating, and second, a *tan h* layer that generates new candidate values (C'_t) potentially added to the cell state. Eq. (2) and Eq. (3)

detail the input gate's parameters.

$$I_t = \sigma\{W_i(h_{t-1}, x_t)\} \tag{2}$$

$$C'_t = tanh\{W_c * (h_{t-1}, x_t)\} \tag{3}$$

The cell state (C_t) undergoes modifications based on several factors, including the forget gate outputs (f_t), the previous cell state (C_{t-1}), the input gate (I_t), and the candidate cell state (C't). Eq. (4) outlines the specific process for updating the cell state:

$$C_t = (f_t * C_{t-1}) + C_t * C'_t \tag{4}$$

The hidden state (h_t) is determined by multiplying the current cell state (C_t), after it has been processed through the tanh activation function, by the output gate (O_t). Eq. (5) provides the mathematical representation of this computation:

$$O_t = \sigma\{W_o.(h_{t-1}, x_t) \tag{5}$$

$$h_t = O_t * tanh\,(C_t) \tag{6}$$

In the equations provided, the recurrent weights (W_f, W_i, W_c, W_o) are responsible for encoding the memory and relationships in the LSTM. These equations describe the dynamic interactions at each time step t involving input x_t, hidden state h_t, and cell state C_t. At the previous time step $t-1$, the corresponding values were represented as h_{t-1} and C_{t-1}. The sigmoid activation function, denoted as σ, is consistently employed across these equations. Specifically, σ represents the input gate, f_t represents the forget gate, O_t represents the output gate, x_t is the input at the current time step, h_t signifies the hidden state at that step, C_t reflects the current cell state, C'_t represents the candidate cell state at time step t, and C_{t-1} denotes the previous cell state. These equations capture the intricate computations that underlie the updates to the cell state and the generation of the hidden state within an LSTM cell.

C. STRUCTURE OF BI-LSTM

A widely employed recurrent neural network (RNN) in the realm of time series forecasting and sequence classification is the bidirectional long short-term memory (Bi-LSTM) model. Designed to adeptly process sequential data, the fundamental structure of the Bi-LSTM model is illustrated in Fig. 3. In this depiction, a sequence of input data is fed into the Bi-LSTM architecture through the input layer. The core of the architecture comprises two LSTM modules, forming the bidirectional LSTM layer. This unique layer processes the input sequence both in the conventional forward direction and simultaneously in reverse, effectively capturing dependencies from both past and future inputs. This configuration enhances the model's ability to discern intricate relationships within the data. To counteract overfitting during the training phase, a dropout layer follows the bidirectional LSTM layer, intermittently deactivating a fraction of units. The output from the LSTM layer is then channeled to the dense layer, constituting the fourth layer, where it undergoes linear transformation to yield the final output. This layer can also incorporate activation functions and regularization techniques, enhancing model performance. Techniques such as grid optimization can be employed to fine-tune model parameters, including the number of LSTM components, layers, and dropout frequencies. Crucially, the process of updating the model during training involves backpropagation through time (BPTT), which takes into account the sequence of previous inputs and outcomes, as depicted in Fig. 3.

D. MATHEMATICAL EXPLANATION OF BI-LSTM

Eq. (7) outlines the input gate's operation within a bidirectional long short-term memory (Bi-LSTM) model. It entails computing a balanced adding of the input x_t, the hidden state from preceding h_{t-1}, and a term related to bias b_i. All three of these components undergo multiplication with their respective learned weight matrices W_i and U_i. The resulting products are subsequently summed together. Finally, function of sigmoid σ is employed to determine the range of the input gate, which is applied to the aforementioned sum to produce the result [32].

$$i_t = \sigma(W_i\,(x_t) + U_i(h_{t-1}) + b_i \tag{7}$$

At time step t, the gate's input column represents the activation of the gate, while x_t denotes the input vector, and h_{t-1} signifies the state that is hidden at the $t-1$ previous time step. The input gate's weighted matrix W_i operates on x_t, the input and the weighted matrix for the state of hidden, W_i, acts on h_{t-1}. b_i as bias term contributes to the input gate. Moving on to Eq. (8), it delineates that how the forgotten gate operates within a Bi-LSTM model. This gate calculates an input x_t sum that is weighted, preceding state of hidden h_{t-1}, and term related to bias b_f. The corresponding weighted matrices W_f as well as U_f have been multiplied by all three of these factors. The resulting products are subsequently summed together. Ultimately, the function of sigmoid σ to the sum is applying to determine the result of the forgotten gate, denoted as f_t.

$$f_t = \sigma(W_f\,(x_t) + U_f\,(h_{t-1}) + b_f \tag{8}$$

At time step t, f_t the forgotten gate column represents the activation of gates, while x_t denotes the input vector. At $t-1$ time step the state of hidden denoted as h_{t-1}, and the weighted matrices for the forgotten gate are W_f and U_f, respectively and they have been assigned to the input as x_t and state of hidden as h_{t-1}. The term related to bias for the forget gate is b_f. Moving on to Eq. (9), it illustrates the Bi-LSTM network calculation of the potential state for cell memory. The potential state of a cell memory c'_t is produced by applying the (tan h) tangential function by hyperbolic upon the resulting matrix after adding the sums of weights and bias.

$$c'_t = tan\,h(W_a\,(x_t) + U_a\,(h_{t-1}) + b_a) \tag{9}$$

At time step t, the potential activated vector c'_t represents the activation, while x_t denotes the input vector. At $t-1$ time step the state of hidden is denoted by h_{t-1}. W_a and U_a are the weighted matrices for potential activated, assigned

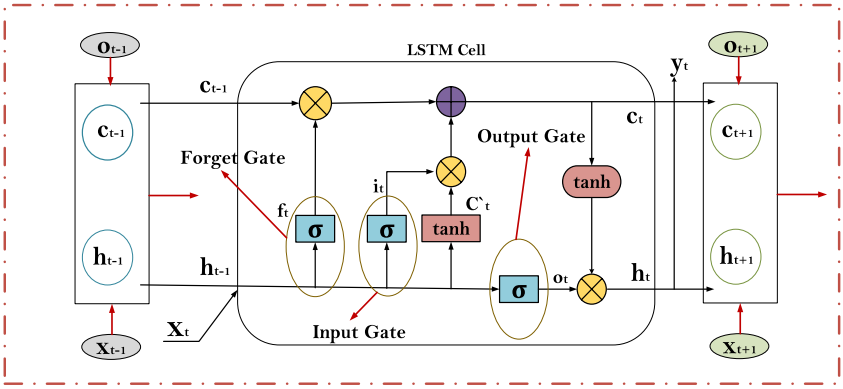

FIGURE 3. Bi-LSTM internal structure.

to the input x_t and state of hidden h_{t-1}, respectively. The term related to bias for potential activation is b_a. Shifting to Eq. (10), it presents the Bi-LSTM model's computation for the cell's state at a unique time step t. Whatever data from the previous state of the cell ought to be kept or left behind is decided by the forget gate f_t. Every bit of data obtained from the preceding state of the cell is lost if the forgotten gate output f_t equals 0, but is retained if f_t equals 1. Subsequently, via the gate for input, fresh information is incorporated into the state of cell's, determining which components of the potential state of the cell c'_t should be retained. Nothing fresh information is included if the input value of the gate is 0, and all fresh information is retained once it equals 1. The state of the cell c_t for the present time step t is updated by combining the both components.

$$c_t = (f_t * c_{t-1}) + i_t * c'_t \tag{10}$$

In Eq. (10), the terms c_t and c_{t-1} refer to the state of cell vectors at time steps t and $t-1$, respectively. At time step t, the input of the gate matrix it and the forgotten gate matrix f_t are both used. Additionally, at time step tc'_t stands for the potential activation matrix. Moving on to Eq. (11), the final state o_t at each step-in time t is calculated. The learnable parameters W_o, U_o, and b_o, along with the most recent input x_t, the prior state of hidden h_{t-1}, define this output state. These factors, which are learned during training, are used to balance and mix the input and the prior state of hidden in order to determine the ultimate outcome state.

$$o_t = \sigma(W_o\,(x_t) + U_o\,(h_{t-1}) + b_o \tag{11}$$

The given input vector, x_t, at each step-in time t determines the resultant gate vector, o_t. The symbol for the state of hidden at each step-in time $t-1$ is h_{t-1}. When applies on the input x_t and the state of hidden h_{t-1}, W_o also U_o are the weighted matrices for the resultant gate, respectively. b_o stands for the output gate's bias term in addition. Moving to Eq. (12) is then used to get the state of hidden, h_t, for each step-in time t. The resultant state, o_t, and the memory state of cell, C^t, serve as the foundation for this computation. The earlier state of hidden, h_{t-1}, and the present input, x_t, are used to calculate the memory state of cell. The state of output is then established using the present state of hidden, h_t, and is used for filtering information from the state of memory cell in a certain manner.

$$h_t = (o_t) * \tan h\left(C^t\right) \tag{12}$$

In the equation, h_t denotes the state of hidden, o_t represents the resultant gate, and C^t signifies the memory state of cell at each step-in time t [32].

E. STRUCTURE OF HYBRID AE-LSTM

The concepts of autoencoders and LSTM (Long Short-Term Memory) networks are combined in an autoencoder LSTM. One specific type of neural network structure, called an "autoencoder," is taught to recreate the data being input by "encoding" it in a simplified form. The autoencoder framework shown in Fig. 4 incorporates LSTM cells, which allows the model to capture temporal relationships and produce useful representations for data that is sequential. The encoder component's LSTM cells handle the ordered input, capturing time relationships and creating a condensed form known as the "encoding" or "latent space." This encoding often represents the data more effectively than the input sequence since it has fewer dimensions. The LSTM decoder is then given the encoded data. The decoder LSTM cells reconstruct the original input sequence by generating an output sequence. The decoder makes an effort to minimize the error of reconstruction by comparing the original input with the reconstructed output as little as feasible. The collection of input sequences is used to train the autoencoder LSTM. The goal is to lessen the disparity among the input sequences and the outputs of their reconstruction. In order to minimize the disparity among the original and reconstructed data, a function of loss, such as the mean-squared error (MSE) or bi cross-entropy loss, is usually used to achieve this. The autoencoder LSTM may be used for compression and reconstruction tasks once it has been trained. The encoder makes a compressed version (encoding) of a new input sequence, while the decoder extracts the original sequence from the encoding. As a result, the input sequence may be compressed into a lower-dimensional

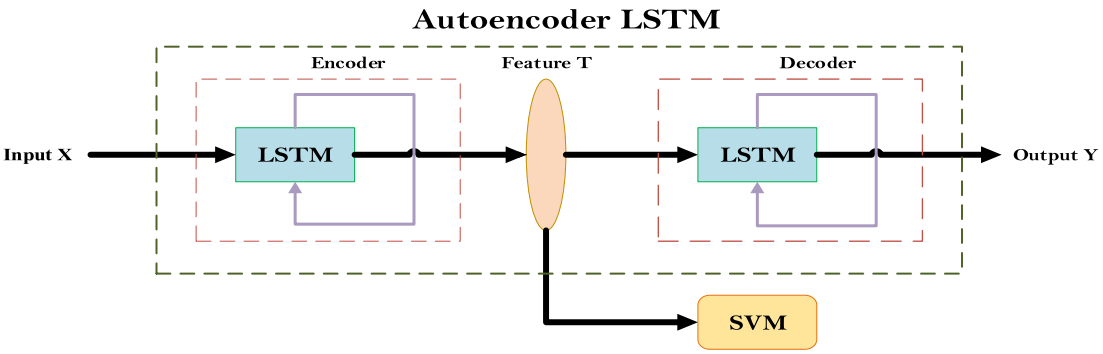

FIGURE 4. Structure of hybrid autoencoder LSTM.

structure and reliably and efficiently reconstructed using the model. Autoencoder LSTM models are particularly suitable for tasks like sequential prediction, finding anomalies, and extraction of features from sequential data because they combine the strengths of LSTM networks in capturing temporal relationships with the compression skills of autoencoders. The model gains the ability to recognize the fundamental patterns of the input sequence, extract significant information from it, and properly recreate it.

F. MATHEMATICAL EXPLANATION OF HYBRID AE-LSTM

The autoencoder is typically used to gather dimensions or features. Let $X = \{x_1, x_2, \ldots, x_k\}$, wherein $x_i \in R^d$ indicates the first input series of data. To ascertain the distinctive layout of the starting data, the function f is used. The series $T = \{t_1, t_2, \ldots, t_k\}$, wherein $t_i \in R^l$ is the sequence that identifies the first series as x. The encoder's output is used as the decoder's input. The decoder reconstructs the original data with regard to the characteristic sequence T. Reconstructed data is represented as $Y = \{y_1, y_2, \ldots, y_k\}$, with $y_i \in R^d$. The collected characteristics are validated by decoding. When the autoencoder's training is complete, its encoder is only used to acquire the original data's attributes, improving data within the organization. The Eq. (13) and Eq. (14) for encoding and decoding are as follows [33]:

$$t_i = f(w_t.x_i + b_t) \tag{13}$$

$$y_i = g(w_y.t_i + b_y) \tag{14}$$

here w_t and w_y stand for weights, b_t and b_y for biases, and $f(\,)$ and $g(\,)$ for sigmoid functions. The initial equation is used in an autoencoder to calculate the state of hidden f_t before the start of the procedure. This requires merging the input x_t, extra data z_t, and the final concealed state h_{t-1} through a weighted sum. The equation of sigmoid is then used to introduce nonlinearity to the resultant sum. The second equation computes the input gate i_t by averaging the inputs and the most recent state of hidden, then using the sigmoid function for further processing the results. Next, the candidate state of cell C_t is obtained by applying an average to the inputs, additional information, and the previous hidden state. The outcome sum is after which it underwent the hyperbolic function of tangent.

$$C'_t = tanh\{W_c * (h_{t-1}, x_t)\} \tag{15}$$

$$O_t = \sigma\{W_o.(h_{t-1}, x_t) \tag{16}$$

Eq. (15) merges the previous state of the cell C_{t-1} with the potential state of the cell C'_t based on the forgotten gate's worth f_t and also gate of input i_t to reflect the C_t state of the cell at each step-in time t. While the forgotten gate determines whatever information from the cell's previous state needs to be kept, the gate of input controls the influence on the candidate state. Eq. (16) calculates the output gate o_t by averaging the inputs and the most recent state of hidden before sending it via the sigmoid function.

$$f_t = \sigma(w_{f1}.x_t + w_{f2}.z_t + wf_3.h_{t-1} + b_f) \tag{17}$$

$$i_t = \sigma(w_{i1}.x_t + w_{i2}.z_t + w_{i3}.h_{t-1} + b_i) \tag{18}$$

$$C'_t = tanh(w_{c1}.x_t + w_{c2}.z_t + w_{c3}.h_{t-1} + b_c) \tag{19}$$

$$C_t = f_t.C_{t-1} + i_t.C'_t \tag{20}$$

Applying the state of cell C_t to deduce the final state of hidden results in the state of hidden h_t. The hyperbolic function of tangent changes the result to produce the final hidden state, while the process of multiplication specifically collects pertinent information from the state of cell. The autoencoder can execute encoding and decoding processes, efficiently compressing and recreating input data, with the help of these equations.

$$o_t = \sigma(w_{o1}.x_t + w_{o2}.z_t + w_{o3}.h_{t-1} + b_o) \tag{21}$$

$$h_t = o_t.tan\,h(C_t) \tag{22}$$

The features of the data covering upstream as well as downstream movements of traffic are captured by the representation z_t. The biases (b_f , b_i, b_c, b_o), and recurrent weights (W_f , W_i, W_c, W_o) used in the computations. The current input x_t, the features of the preceding and succeeding steps z_t, and also h_{t-1} the final state of the unit, make up the input for the forget gate. C_t and C_{t-1} are used to designate the cell states at each step-in time t and *t-1*, respectively. The activation function is the sigmoid function, which is frequently denoted by the symbol σ. A piece of the cell's state from the previous phase is now removed, and a portion is added. The

output gate's data from input is similarly equivalent to that of the forgotten gate. The gate for output selects the information that must be output. The tanh function, which has completed analyzing the state of the cell [33], multiplied this result.

In our proposed framework, the enhanced input data undergoes the training phase, which comprises two distinct sections, a hybrid model that combines Autoencoder and Long Short-Term Memory (AE-LSTM). The hybrid model as shown in Fig. 4, our propose hybrid AE-LSTM to predict three critical parameters: ''Daily power generation'', ''Maximum grid-connected power generation'', and ''Radiance''. The hybrid AE-LSTM model developed for solar power prediction combines the memory capabilities of LSTM networks with the feature extraction functionality of Autoencoders. This combination aims to enhance prediction accuracy by effectively grasping the intricate temporal patterns and correlations present in solar power generation data. To achieve this, the model follows a sequence of steps: the initial preparation of raw solar power data, the extraction of key features using an autoencoder, which compresses essential data elements into a condensed form, and the subsequent utilization of this compressed representation by the LSTM component. The LSTM processes this representation in a step-by-step manner, capturing the underlying temporal relationships. Moreover, standard LSTMs struggle with learning temporal dependencies across sequences. To overcome these challenges, we devised a hybrid architecture to develop a robust solution for precise power prediction. Through training and validation on historical data, the hybrid AE-LSTM model becomes skilled at forecasting future solar power generation values, making use of the insights derived from the extracted features and temporal dependencies. While a basic LSTM model performs well, it falters in capturing temporal dependencies between sequences. In contrast, AE-LSTM effectively learns such dependencies. This empirical evidence is discussed in section IV. As a result, we assert that our hybrid Autoencoder LSTM model yields impressive outcomes, surpassing even the Bi-LSTM model in terms of performance and effectiveness.

III. CASE STUDY

A. SOLAR PLANT'S STRUCTURE

In Chakwal, Punjab, Pakistan, there is a notable 100 MW solar plant called the Sapphire Solar Power Plant (SSPP). The Sapphire Group, a well-known Pakistani corporation with diverse holdings in textile production, electricity generation, and property development, built this remarkable plant. The installation, which spans a vast area of over 650 acres, impressively contains over 400,000 solar panels. The National Transmission and Dispatch Company (NTDC) painstakingly built a 132 kV transmission line that efficiently connects the SSPP to the national grid. Since it began doing business in April 2018, the SSPP has faithfully performed its duties by producing clean and renewable energy to meet Pakistan's rising energy needs. With an estimated 165 GWh of yearly power production, the plant significantly lessens Pakistan's dependency on energy from fossil fuels and actively aids in the country's attempts to tackle global warming. The SSPP's successful development and operation represent an important turning point for Pakistan's renewable energy industry, demonstrating unequivocally the viability and potential of large-scale solar power projects there.

TABLE 1. Installed equipment detail.

Detail of Equipment	No.	Units
Type of Substation	1	AIS
Plant's Capacity	100	MW
No. of Solar Panels	400,000	330Wp
Combiner's Box	1500	DC
Inverter	250	500Kw
Auxiliary Transformer	120	0.315/33kV
Feeder	20	132kV
Main Transformer	02	132kV-100MVA
SVC (Static Var Compensators)	02	-5~+15 MVAR

B. INSTALLED EQUIPMENT DETAILS AT SOLAR PLANT

The following provides thorough details about the installed equipment, with Table 1 serving as a guide.

Solar Panels: An astonishing network of over 400,000 solar panels, each with a 330-watt capacity, is installed at the solar power plant. Trina Solar, a well-known solar panel maker with its head office in China, is the source of these solar panels.

Inverters: The facility uses centralized inverters made by Sungrow, a major Chinese business famous for creating high-quality solar inverters, to efficiently convert the DC power generated by the solar panels into AC electricity that is acceptable for the grid.

Mounting Structures: The solar panels are firmly secured to fixed-tilt mount systems that have been meticulously engineered to maximize energy output by optimizing panel angle. These mounting structures are produced by Array Technologies, a reputable supplier of solar tracking systems.

Transformers: The power plant uses step-up transformers to raise the voltage of the energy produced by the solar panels before putting it into the grid. These transformers are produced by Siemens, a well-known provider of power-related goods and services.

Switchgear: The switchgear at the power plant is carefully planned to guarantee the electrical equipment's security and dependability. The switchgear is produced by ABB, a prominent manufacturer of power and automation technology.

Monitoring and Control System: Through an elaborate monitoring and control system, the power plant uses cutting-edge technology to allow operators to remotely monitor the performance of equipment and maximize energy output. This cutting-edge monitoring and control system is provided by Huawei, a top supplier of information and communications technology services.

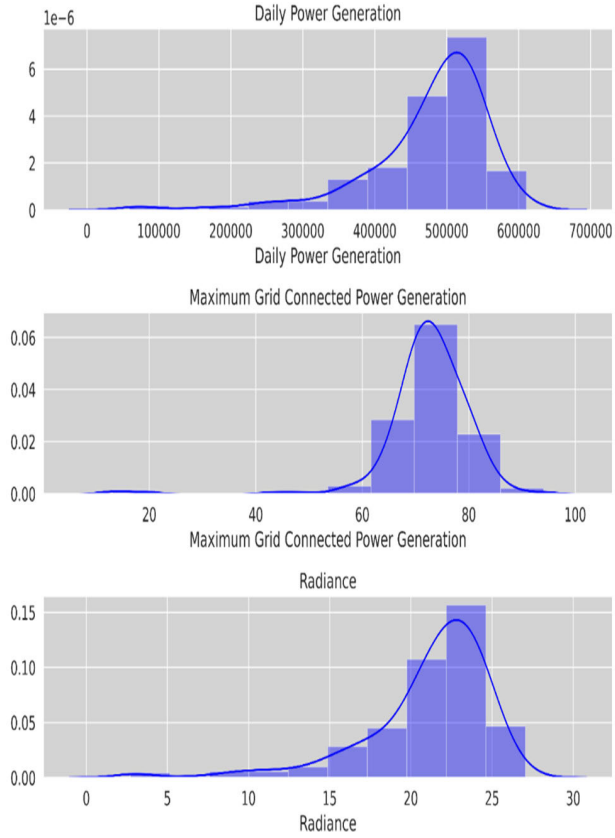

FIGURE 5. Data analysis of solar plant parameters via a histogram.

C. DATA ANALYSIS

A histogram is a valuable analytical tool used to examine the characteristics of a dataset, where the curve is known as distribution curve. By displaying the frequency distribution of data, it can reveal outliers, trends like normal distribution, and compute statistical measures such as mean, median, and standard deviation. Moreover, it unveils peculiar patterns and offers a clear and straightforward representation of data distribution, enabling easy comparison of different datasets and uncovering insights not readily apparent from raw data alone. The histogram's organization of data is akin to that of a pie chart.

In Fig. 5, the ''Daily Power Generation'' section of the histogram illustrates the flow of daily solar electricity production. The x-axis shows the quantity of units produced in bins of 0 kWh to 700,000 kWh, while the y-axis depicts unit showing frequency, which ranges from 0. to 8. Similarly, the histogram for ''Maximum Grid-Based Power Generation'' displays the maximum grid-based power generation frequency, with scores ranging between 0.00 to 0.06, and the x-axis representing power generation values in bins of 0 to 100 MW. It also depicts the variation in power generation values over time via calculating frequencies of maximum grid-based power values in each and every bin, displayed on the y-axis. For the ''Radiance'' histogram, the y-axis runs between 0.00 to 0.15, while the x-axis found between 0 to 30 MJ·m^{-2}. The x-axis represents radiance values at 1-width intervals, with the final interval being from 29 to 30 MJ·m−2. The histogram's form sheds light on how the radiance readings are distributed. The right side as the histogram tilts, it indicates a higher frequency of low radiance scores, whereas a tilt towards the left signifies a higher frequency of high radiance scores. If the histogram is symmetrical, it indicates a uniform radiance distribution.

Box plots provide a concise and informative summary of extensive datasets, offering insights into their distribution. Fig. 6 showcases box plots representing three features extracted from a substantial solar power facility: ''Daily Power Generation'' (measured in kWh), ''Maximum Grid Connected Power Generation'' (measured in MW), and ''Radiance'' which is measured in MJ·m^{-2}. The vertical extent of each box displays the data's middle 50%, with the lines extending from the box indicating the minimum and maximum values falling inside the range that is interquartile by 1.5 times. Any data points beyond these intervals appears as separate dots or circles as well, which may indicate potential significant anomalies.

In the first box plot, ''Daily Power Generation in kWh,'' displays the interval of generated units on the y-axis, spanning from 100,000 kWh to 600,000 kWh. First quartile (Q1) covers the range from 330,000 to 450,000, representing the data's lowest 25%. The second quartile (Q2) ranges from 450,000 to 500,000, signifying the midpoint of the data, or 50%. Third quartile (Q3) encompasses the range from 500,000 to 530,000, representing the upper 25% of the data. Finally, the fourth quartile (Q4) spans from 530,000 to 610,000, indicating that this interval includes the top 1% of the data.

The box plot in second, ''Maximum Grid Connected Power Generation in MW,'' displays the power generation range from 10 MW to 90 MW on y-axis. Q1 runs between 60 to 70, indicating the bottom 25% of the data. Q2 covers the range from 70 to 73, representing the midpoint of the data, or 50%. Q3 encompasses the interval from 73 to 78, signifying the upper 25% of the data. Lastly, Q4 ranges from 78 to 88, indicating this interval includes the top 1% of the data.

The last box plot, ''Radiance,'' presents the power generation found between 5 MJ·m^{-2}- 30 MJ·m^{-2} on y-axis. Q1 spans from 14 to 20, representing the bottom 25% of the data. Q2 ranges from 20 to 22.5, signifying the middle 50% of the data. Q3 encompasses the range from 22.5 to 23.5, representing upper 25% of the data. Finally, Q4 ranges from 23.5 to 27, indicating that this interval includes the top 1% of the data, as depicted in Fig. 6.

The heat map shown in Fig. 7 provides a visual representation of the correlation between the three parameters. The heat map consists of three columns and three rows, where the correlation value among any two parameters is shown in each of the cells. The cells that are diagonal show how closely every parameter is correlated by itself, resulting in a correlation coefficient of 1, indicating perfect correlation. The correlation coefficient values within the cells range from 0 to 1. Higher values indicate a stronger positive correlation

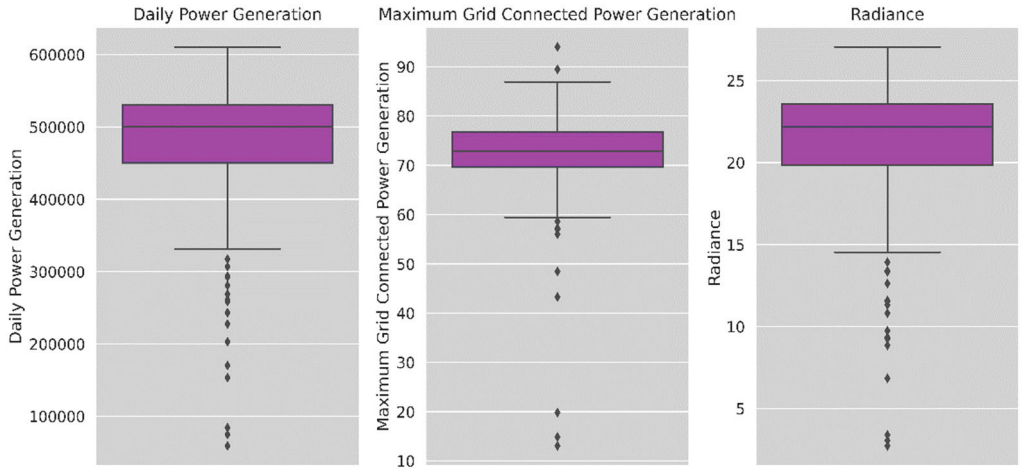

FIGURE 6. Data analysis of solar plant parameters via box plot.

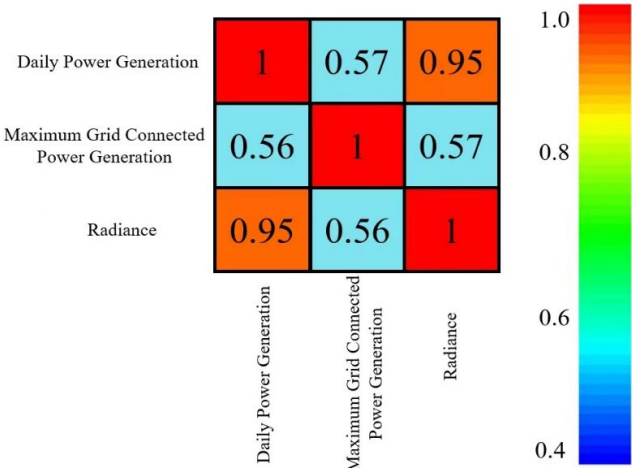

FIGURE 7. Data analysis of solar plant parameters via a heat map.

between the two parameters, while lower values suggest a weaker or negative correlation. A correlation coefficient of 1 represents an absolute positive correlation, indicating that the two parameters move in perfect harmony. On the other hand, a coefficient of 0 signifies no correlation, meaning the two parameters are independent of each other. A coefficient of -1 indicates an absolute negative correlation, indicating that the two parameters move in opposite directions. To aid interpretation, the right side's color bar of the heat map represents the range of correlation coefficients. The color bar spans from 0.6 to 1.0, with darker colors representing higher positive correlation values, while lighter colors indicate lower positive correlation values. The color intensity provides a visual clue to the strength of the correlation between the parameters.

In next section IV, results acquired from both the models are discussed in graphical visualization form.

IV. RESULTS AND DISCUSSION

In this study, a solar power plant provided a one-year database that included real-time data for three parameters: ''daily power generation (kWh)'', ''grid-connected power generation (MW)'', and ''radiance ($MJ \cdot m^{-2}$)''. These parameters were used to predict the ''daily power generation, grid-connected power generation, and radiance'' for the following year. To achieve this, three distinct models were employed: the long short-term memory (LSTM) model, bidirectional long short-term memory (Bi-LSTM) model and the Hybrid Autoencoder LSTM (AE-LSTM) model. These models were chosen after a thorough assessment of the literature that demonstrated their effectiveness for this goal and their accuracy. The outcomes from the models show good agreement between forecasts and the findings of the genuine real-time data. However, through graphical visualizations and a comparison table, it is evident that the hybrid Autoencoder LSTM model outperformed the LSTM as well as Bi-LSTM model. The Autoencoder LSTM exhibited a lower error rate and significantly improved prediction accuracy. This section presents the results, tables, and graphical visualizations obtained from these models, emphasizing the remarkable advancements achieved by the Autoencoder LSTM.

Table 2 provides valuable insights into the hybrid model's architecture and parameters. The model consists of multiple

TABLE 2. Hybrid model sequential steps for prediction.

Layer (type)	Output Shape	Param #
lstm_105 (LSTM)	(None, 4, 10)	480
lstm_106 (LSTM)	(None, 4, 6)	408
lstm_107 (LSTM)	(None, 1)	32
repeat_vector_21 (Repeat Vector)	(None, 1, 1)	0
lstm_108 (LSTM)	(None, 1, 10)	480
lstm_109 (LSTM)	(None, 1, 10)	840
dense_21 (Dense)	(None, 1, 1)	11

Total params: 2,251
Trainable params: 2,251
Non-trainable params: 0
None
dict_keys(['loss', 'mse', 'mae'])

layers, each with distinct roles in data processing. The "Output Shape" column specifies the dimensions of the output produced by each layer. For example, the first LSTM layer (lstm_105) generates outputs with a shape of (None, 4, 10), indicating a batch size of none, sequence length of 4, and feature dimension of 10. Similarly, the subsequent LSTM layers (lstm_106 and lstm_107) have output shapes of (None, 4, 6) and (None, 1), respectively. The "Param #" column provides the number of trainable parameters for each layer, including weights and biases. In this model, lstm_105 has 480 parameters, lstm_106 has 408 parameters, lstm_107 has 32 parameters, repeat_vector_21 has no parameters as it is a repeating layer, lstm_108 has 480 parameters, lstm_109 has 840 parameters, and dense_21 has 11 parameters. There are 2,251 parameters that can be trained in the model, all of which are trainable. Additionally, the table highlights the absence of non-trainable parameters in this specific model. The dictionary keys listed in the table, such as 'loss', 'mse', and 'mae', represent various loss metrics used for training and evaluating the effectiveness of model. Metrics like Mean Squared Error (MSE) and Mean Absolute Error (MAE) assist in assessing the model's effectiveness. Overall, Table 2 offers crucial details about the hybrid model's architecture.

The dataset consists of data which are available in real-time values collected over one year. 80% of the dataset is used for training the LSTM (long short-term memory) model, Bi-LSTM (bidirectional long short-term memory) model and the hybrid AE-LSTM (Autoencoder long short-term memory) model, while the remaining 20% is reserved for testing and validation. The losses obtained from both models are compared and graphically visualized.

In Fig. 8(a-c), the validation loss results for the parameters "daily power generation," "grid-connected power generation," and "radiance" from the solar power plant are depicted for models LSTM, Bi-LSTM and hybrid AE-LSTM. Seeing that, the LSTM and Bi-LSTM model's validation loss results are acceptable, but the AE-LSTM model shows significantly lower losses. Table 3 provides a detailed comparison of losses for both models. The AE-LSTM model achieves the lowest loss of 0.018571 for "daily power generation (kWh)," outperforming Bi-LSTM model with a loss of 0.022655 and LSTM model with validation loss of 0.04876. Similarly, for "grid-connected power generation," the AE-LSTM model achieves the lowest validation loss of 0.008305, compared to Bi-LSTM model's loss of 0.008836 and LSTM model loss of 0.01936. Lastly, for "radiance," the AE-LSTM model attains a minimum validation loss score of 0.019438, during this time the Bi-LSTM and LSTM model's score is 0.022582 and 0.03714 respectively. However, the validation loss of all these models is acceptable but these findings unequivocally show that hybrid AE-LSTM model surpasses both the LSTM and Bi-LSTM model in terms of minimizing losses. The graphical representations in Fig. 8(a) through (c) also demonstrate the absence of anomalies within the data. Moreover, the recorded errors signify a high level of accuracy, exceeding 95% precision. This suggests that the data is well-balanced, indicating an appropriate suitability for subsequent analysis and prediction.

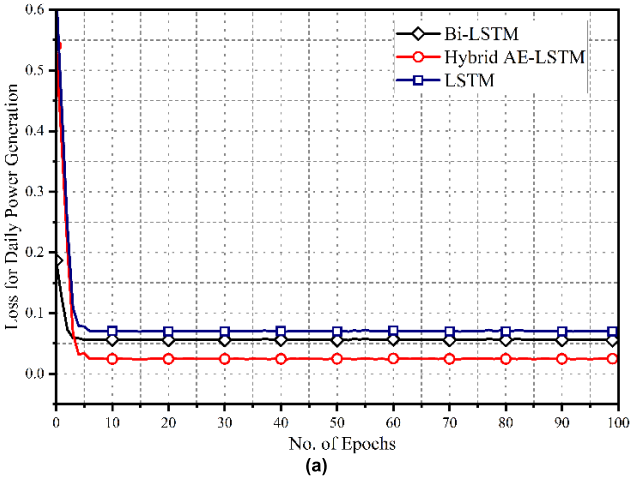

FIGURE 8. Losses comparison (a) Daily power generation; (b) Grid-connected power generation; and (c) Loss of radiance.

Similarly, to compute the Mean Absolute Error (MAE) for a machine learning model and assess the absolute variance between the predicted and true scores of the target variable, several steps can be followed. First, obtain the model's predicted values. Next, gather the true values of the target variable from the dataset or ground truth. Then, calculate the absolute difference among them. Finally, calculate the average of all these absolute differences to obtain the MAE result. A low MAE score suggests that the predictions made by the model are more accurate, being closest to the true scores. The mathematical expression of the Mean Absolute Error (MAE) is represented by Eq. (23).

$$MAE = \frac{1}{N}\sum_{n=1}^{N} |\overline{x_n} - x_n| \tag{23}$$

where $\overline{x_n}$ represents the predicted score, x_n represents the observed score, and N is the number of data points.

Table 3 presents the results of the mean absolute errors (MAEs) comparison between the LSTM (Long short-term memory), Bi-LSTM (bidirectional long short-term memory) model and the hybrid AE-LSTM (Autoencoder long short-term memory) model using the parameters "daily power generation," "grid-connected power generation," and "radiance" from a power plant of solar.

Additionally, Fig. 9(a-c) depict that the hybrid AE-LSTM model achieves significantly lower validation MAE results compared to the LSTM and Bi-LSTM model. Specifically, in Table 3, the AE-LSTM model achieves the lowest MAE values of 0.090133 for "daily power generation (kWh)," 0.056495 for "grid-connected power generation," and 0.094229 for "radiance." In contrast, the Bi-LSTM model scores 0.106682, 0.0554, 0.102336 while LSTM model scores 0.111165, 0.06098, 0.10792 for "daily power generation (kWh)," "grid-connected power generation, (MW)" and "radiance (MJ/m^2)" respectively. These results clearly indicate that the AE-LSTM model outperforms both the models in minimizing MAE. The results emphasize the improved effectiveness and performance of the hybrid Autoencoder LSTM model in capturing the fundamental patterns and generating more precise forecasts for the power generation of the solar plant. Fundamental patterns and generating more precise forecasts for the power generation of the solar plant.

In Fig. 10(a-c), the results of validation mean squared error (MSE) between the LSTM, Bi-LSTM and hybrid AE-LSTM models are compared using the parameters "daily power generation," "grid-connected power generation," and "radiance" from a solar power plant. As shown, all the models MSE results are acceptable but the AE-LSTM model's MSE results are significantly lower. Moreover, in Table 3, the AE-LSTM model achieves the lowest MSE of 0.018571 for "daily power generation (kWh)," while the Bi-LSTM model has an MSE of 0.022655 and LSTM model has 0.04876. For "grid-connected power generation (MW)," the AE-LSTM model achieves the lowest MSE of 0.008305 compared to the Bi-LSTM model's 0.008836.

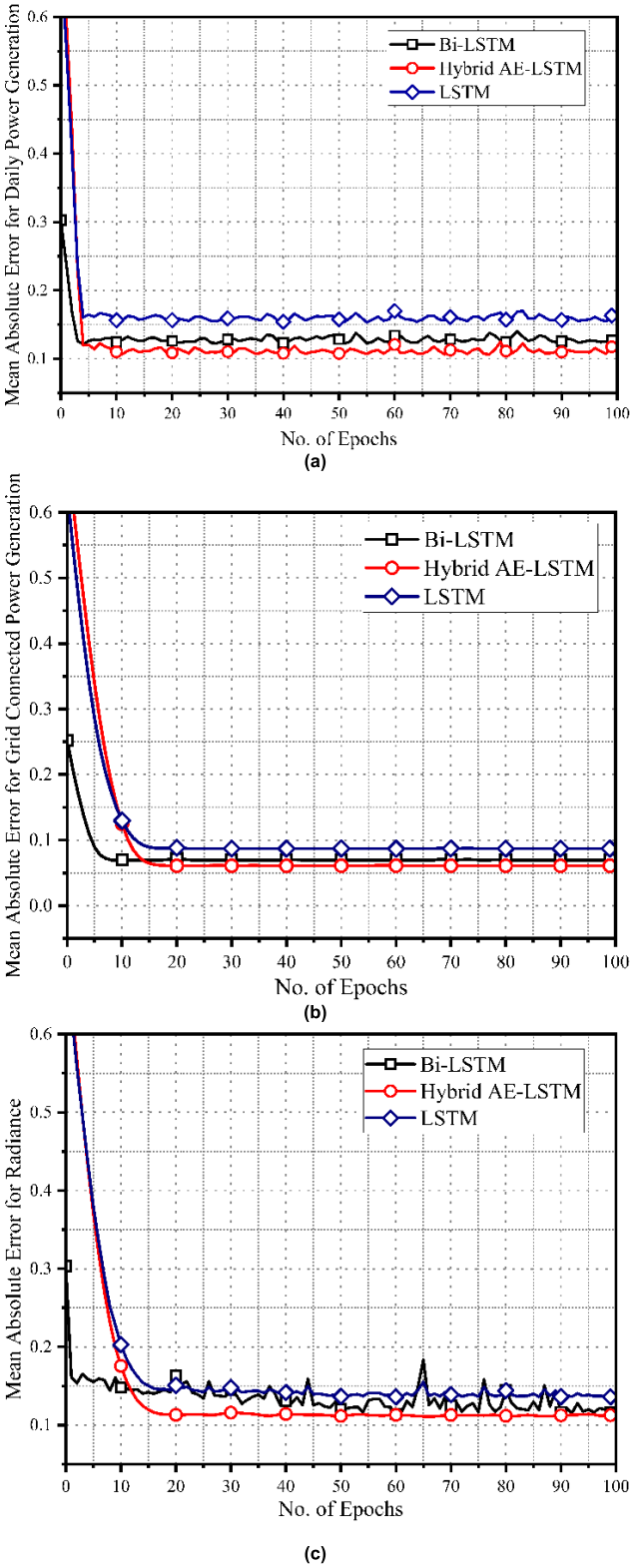

FIGURE 9. MAE comparison (a) Daily power generation; (b) Grid-connected power generation; and (c) Loss of radiance.

Similarly, for "radiance (MJ/m^2)," the AE-LSTM model obtains the lowest MSE of 0.019438, while the Bi-LSTM model scores 0.022582 and LSTM with slightly high

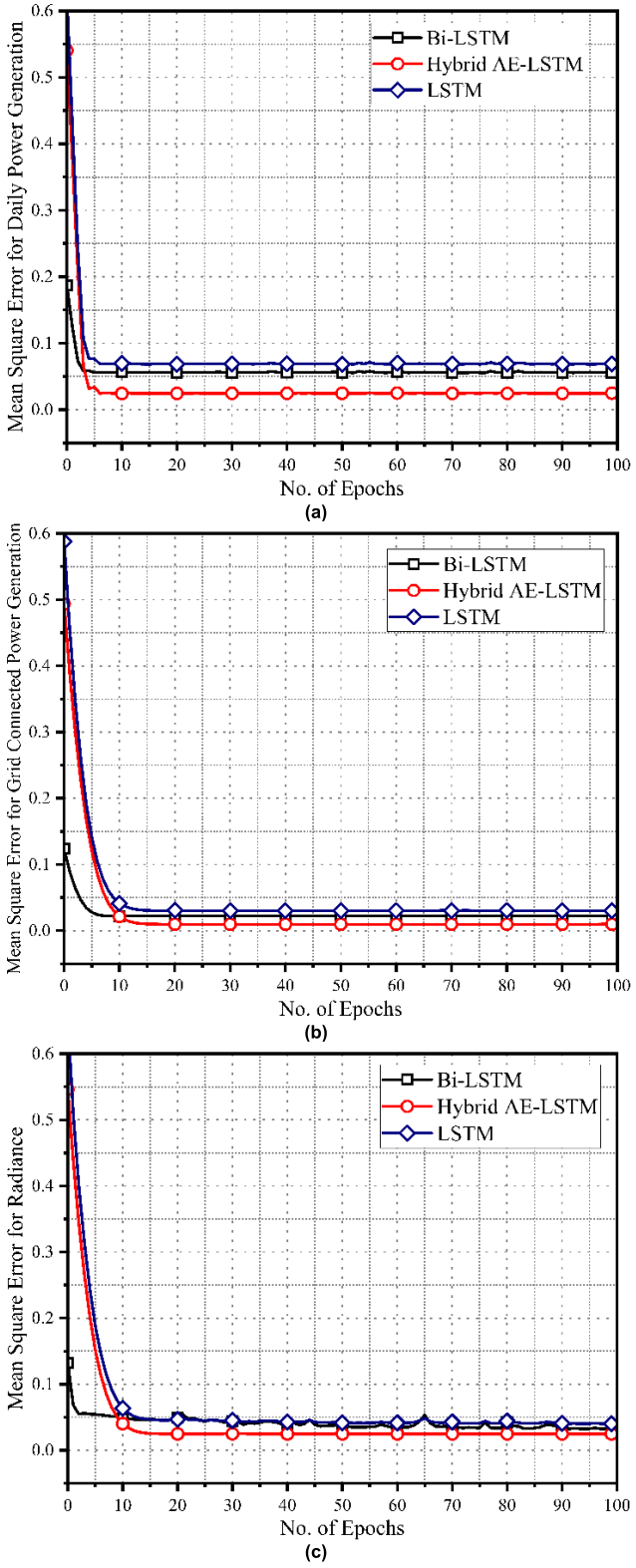

FIGURE 10. MSE comparison (a) Daily power generation; (b) Grid-connected power generation; and (c) Loss of radiance.

0.03714. These results clearly demonstrate that the AE-LSTM model surpasses the Bi-LSTM as well as LSTM model in minimizing MSE.

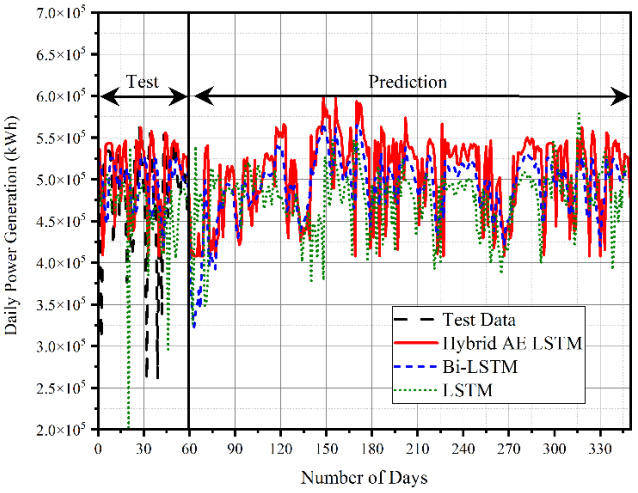

FIGURE 11. Comparison between tested and predicted data of models on daily power generation of a solar plant.

In a similar manner, to calculate the Mean Square Error (MSE) for a machine learning model and evaluate the squared variance between the predicted scores and the true scores of the target variable, several steps are involved. First, obtain the predicted values from the model. Next, collect the true values of the target variable from the dataset. Then, compute the squared variance between each predicted score and its corresponding true score by subtracting the true value from the prediction and squaring the result. Finally, calculate the average of all these squared differences to obtain the MSE result. The MSE provides insight into the average magnitude of errors made by the model, A low MSE score denotes more precise forecasts from the model and closely aligned with the true scores. The mathematical expression of the Mean Square Error (MSE) is represented by Eq. (24).

$$MSE = \frac{1}{N}\sum_{n=1}^{N}(\overline{x_n} - x_n)^2 \tag{24}$$

where $\overline{x_n}$ stands for the predicted score, x_n for the observed score, and N total number of points of data.

Furthermore, upon analyzing the graphical representations of the models, a high degree of similarity is evident, indicating that the data accuracy exceeds 95%, and no outliers have been identified. These findings further affirm the appropriateness and precision of the data acquired from the solar power plant, establishing a robust foundation for subsequent analysis and decision-making processes.

Fig. 11, 12, and 13 provide graphic representations of forecast results from an analysis given data, exercise carried out on a 100 MW solar power facility. In this study, three machine learning models LSTM (long short-term memory), Bi-LSTM (bidirectional long short-term memory) and hybrid AE-LSTM (autoencoder long short-term memory) were trained on three key parameters using 80% of an entire year of data available in real-time: "daily power generation (kWh)", "grid-connected power generation (MW)", and "radiance (MJ·m^{-2})". An additional data of 20% was

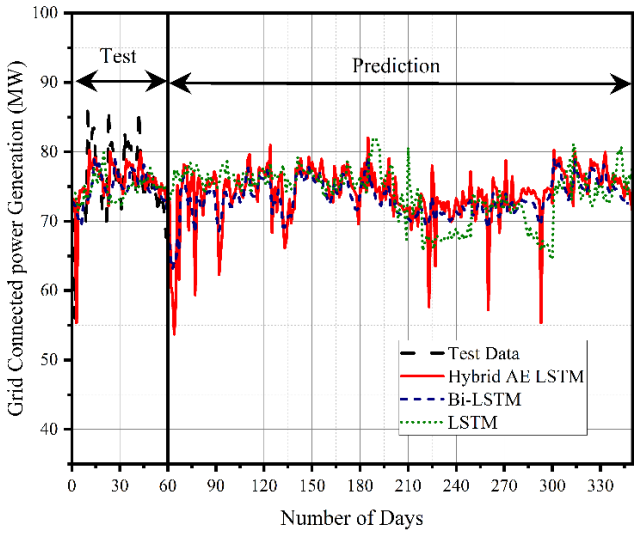

FIGURE 12. Comparison between tested and predicted data of models on grid connected power generation of a solar plant.

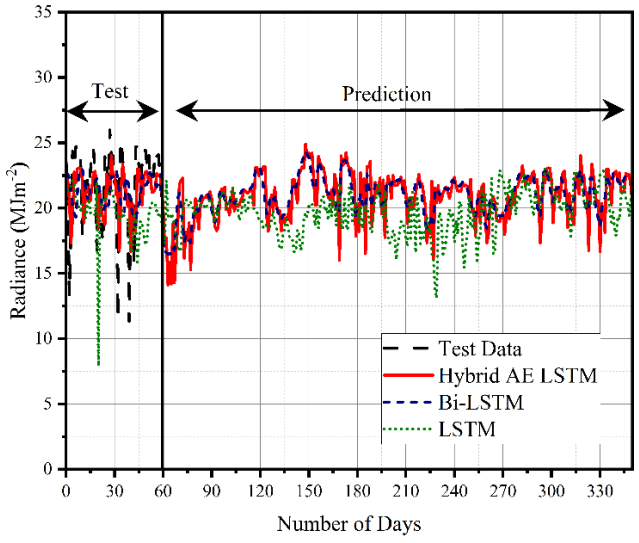

FIGURE 13. Comparison between tested and predicted data of models on radiance of a solar plant.

dedicated for testing and validation. To compare the performance of the two models, a comprehensive analysis was conducted using training data of 10-months and test data of 2-months. Moreover, each of the models produced forecasts for the next year for each of the three parameters. The graphical representations in Fig. 11, 12, and 13 provide an easy-to-read comparison of the findings and forecasts for all three factors in a single graph. The first section of the visuals shows the contrast between the real forecast database and the solar plant's 60-day test data. The solar plant's one-year forecasts for the future are shown in the second section of the graph depending on each parameter. Ideally, the prediction data should closely align with the test data, indicating that the models have successfully captured the true trends and patterns in the solar plant's parameters. The closer the prediction data aligns with the test results, the more accurate the models are in forecasting the values of the parameters.

Table 4 shows the results from Model Confidence Set (MCS). The Model Confidence Set (MCS) is a statistical technique used to assess and compare the accuracy of multiple models for forecasting based on their out-of-sample performance [11]. MCS aims to create a confidence set of models that are statistically indistinguishable in terms of their performance. It relies on statistical tests and p-values to assess the significance of differences in model performance. The term "null hypothesis" is a foundational concept in statistical hypothesis testing. The null hypothesis can be agreed or rejected based on p-values resulting from the models under investigation. In the MCS procedure, the initial step involves considering different models for forecasting. These models may have diverse specifications and assumptions. The final set of models that 'survive' the MCS procedure is determined by the chosen significance level. In the last step, the final confidence set consists of models with p-values greater than or equal to the significance level. In our study, the results of all the models are acceptable, but the Hybrid Autoencoder LSTM model outperforms the Bi-LSTM and LSTM models in terms of our three parameters: "Daily Power Generation", "Maximum Grid Connected Power Generation", and "Radiance".

Fig. 11 displays the range of the "daily generation (kWh)" parameter, whose y-axis spans 200,000 to 700,000 kWh and whose x-axis represents the number of days. The predicted data from the LSTM, Bi-LSTM as well as hybrid AE-LSTM models and the actual 60-day test data can be compared, and it can be shown that the predictions from all these models are in acceptable range but the hybrid AE-LSTM model are well synced with the findings from the test, with just tiny differences at select places. On the other hand, Bi-LSTM and LSTM results do not match the test data closely, likely due to their limited ranges. However, the results of Bi-LSTM are slightly better when compare to LSTM which shows out of range at certain time. The daily generating statistics for the upcoming entire year (365 days) will be predicted using each trained models for prediction after this comparison. Fig. 11 shows that the hybrid Autoencoder LSTM model's predictions are much closer to the test data as compared to Bi-LSTM's and LSTM's results, displaying minimal deviations. As a result, the hybrid Autoencoder LSTM model is highly recommended for its superior performance in accurately forecasting the parameter's values.

Similarly, Fig. 12 represents the "maximum grid-connected power generation (MW)" parameter, y-axis fluctuates between 40 MW to 90 MW, while the x-axis represents the total number of days. The comparison of predicted data using LSTM, Bi-LSTM and AE-LSTM models with the test data of 60-days demonstrates that hybrid AE-LSTM's predictions are well synced with the findings from the test, with just tiny differences at select places. Conversely, Bi-LSTM results do not match the test data closely

TABLE 3. Comparison table between LSTM, Bi-LSTM and hybrid AE-LSTM.

Parameter	LSTM			Bi-LSTM			Hybrid Autoencoder LSTM		
	LOSS	MAE	MSE	LOSS	MAE	MSE	LOSS	MAE	MSE
Daily Power Generation	0.04876	0.111165	0.04876	0.022655	0.106682	0.022655	0.018571	0.090133	0.018571
Grid Connection Power Generation	0.01936	0.06098	0.01936	0.008836	0.0554	0.008836	0.008305	0.056495	0.008305
Radiance	0.03714	0.10792	0.03714	0.022582	0.102336	0.022582	0.019438	0.094229	0.019438

TABLE 4. Models confidence set result.

Parameter	LSTM		Bi-LSTM		Hybrid Autoencoder LSTM	
	RMSE	*p*-MCS	RMSE	*p*-MCS	RMSE	*p*-MCS
Daily Power Generation	0.220817	0.856	0.150514	0.975	0.136277	1.000
Grid Connection Power Generation	0.13914	0.883	0.094002	0.943	0.09113	1.000
Radiance	0.192717	0.879	0.150272	0.972	0.139421	1.000

but better than LSTM results which shows much deviations. The grid-connected power statistics for the upcoming entire year (365 days) will be predicted using each trained models for prediction after this comparison. Upon evaluating the accuracy and performance of the models based on the test and prediction data graphs in Fig. 12, It's clear that the hybrid Autoencoder LSTM model performs better than the other models. The hybrid Autoencoder LSTM model's predictions exhibit closer alignment with the test data, showing minimal deviations and higher accuracy in forecasting the parameter's values.

Finally, Fig. 13 illustrates the "radiance (MJ/m^2)" whose y-axis spans 0 to 30 MJ/m^2 and whose x-axis represents the number of days. The predicted data from the LSTM, Bi-LSTM as well as hybrid AE-LSTM models and the actual 60-day test data can be compared, and it can be shown that the predictions from all the models are acceptable but the hybrid AE-LSTM model are well synced with the findings from the test, with just tiny differences at select places. In contrast, Bi-LSTM results do not closely match the test data. The radiance for the upcoming entire year (365 days) will be predicted using each trained models for prediction after this comparison. Fig. 13 highlights that the hybrid Autoencoder LSTM model outperforms the Bi-LSTM as well as LSTM model, as its predictions closely align with the test data, exhibiting minimal deviations and demonstrating higher accuracy in forecasting the parameter's values.

V. SOFTWARE AND SYSTEM DETAILS

There were certain software and hardware setups used for this study's experimental phase. An Intel(R) Core i7-10875H CPU with a base frequency of 2.30 GHz and an NVIDIA GeForce RTX 2060 graphics card with 6 GB of GPU memory and 16 GB of RAM were the computer components used. A 64-bit version of the Windows operating system served as the foundation for the whole system. Software-wise, the research used the Keras and TensorFlow version 2.12.0 libraries for deep learning modeling, together with the Python 3.11 programming language. These hardware and software sets were carefully chosen, which emphasizes how important they are to assuring the efficacy and accuracy of the research results.

VI. CONCLUSION

The findings of this investigation demonstrate that our proposed Hybrid AE-LSTM (Autoencoder long short-term memory) model outperformed the both Bi-LSTM (bidirectional long short-term memory) as well as LSTM (long short-term memory) model in regards of accuracy and performance measures for each of the parameters. The visual representations provided compelling evidence that the Hybrid Autoencoder LSTM model consistently outperformed the other models in every scenario. However, all these models exhibited expected behaviors, but the Hybrid Autoencoder LSTM model consistently showed lower error rates and higher data similarity. In particular, the daily power generation parameter yielded an RMSE of 0.136 for the Hybrid Autoencoder LSTM model, 0.150 for the Bi-LSTM model and 0.220 for the LSTM model. Similar results were obtained for the grid-connected power generation parameter, where the RMSE for the Hybrid AE-LSTM model was 0.091 and the RMSE for the Bi-LSTM model was 0.094. Last but not least, for the radiance parameter, the AE-LSTM model

outperformed the Bi-LSTM model as well as LSTM model with an RMSE of 0.139 as opposed to 0.150 and 0.192 respectively. These findings show that the Hybrid Autoencoder LSTM model can make more accurate and reliable predictions for these parameters, especially crucial for controlling solar power facilities in an efficient manner.

Future studies should examine the use of additional deep-learning models for power forecasting in time series from renewable sources, such as convolutional neural networks (CNNs) and other hybrid-based models. Additionally, adding more pertinent elements, including information on the grid load and weather, might improve the models' forecasts substantially.

ACKNOWLEDGMENT

Dr. Mohammad Alibakhshikenari acknowledges support from the CONEX-Plus programme funded by Universidad Carlos III de Madrid and the European Union's Horizon 2020 research and innovation programme under the Marie Sklodowska-Curie grant agreement No. 801538. Additionally, Dr. Ashfaq Ahmad sincerely appreciates funding from Researchers Supporting Project number (RSPD2023R666), King Saud University, Riyadh, Saudi Arabia.

REFERENCES

[1] J. Liu, Y. Wang, L. Lu, J. Li, and Y. Qiu, "Review on electrical energy storage system integration and energy management in renewable energy power generation," *J. Mod. Power Syst. Clean Energy*, vol. 7, pp. 1005–1020, Sep. 2019.

[2] R. Asghar, M. H. Sulaiman, S. Saeed, H. Wadood, T. K. Mehmand, and Z. Ullah, "Application of linear and nonlinear control schemes for the stability of smart grid," in *Proc. Int. Conf. Emerg. Technol. Electron., Comput. Commun. (ICETECC)*, Dec. 2022, pp. 1–6.

[3] S. Saeed, R. Asghar, F. Mehmood, H. Saleem, B. Azeem, and Z. Ullah, "Evaluating a hybrid circuit topology for fault-ride through in DFIG-based wind turbines," *Sensors*, vol. 22, no. 23, p. 9314, Nov. 2022.

[4] B. Azeem, Z. Ullah, F. Rehman, S. M. Ali, A. Haider, S. Saeed, I. Hussain, C. A. Mehmood, and B. Khan, "Levenberg–Marquardt SMC control of grid-tied doubly fed induction generator (DFIG) using FRT schemes under symmetrical fault," in *Proc. 1st Int. Conf. Power, Energy Smart Grid (ICPESG)*, Mirpur, Pakistan, Apr. 2018, pp. 1–6.

[5] B. Azeem, F. Rehman, C. A. Mehmood, S. M. Ali, B. Khan, and S. Saeed, "Exact feedback linearization (EFL) and de-couple control of doubly fed induction generator based wind turbine," in *Proc. Int. Conf. Frontiers Inf. Technol. (FIT)*, Islamabad, Pakistan, Dec. 2016, pp. 330–335.

[6] R. Asghar, Z. Ullah, B. Azeem, S. Aslam, M. H. Hashmi, E. Rasool, B. Shaker, M. J. Anwar, and K. Mustafa, "Wind energy potential in Pakistan: A feasibility study in Sindh province," *Energies*, vol. 15, no. 22, p. 8333, Nov. 2022.

[7] A. S. Farag, S. H. Elkholy, and R. E. AlDabbagh, "Integration of artificial intelligence techniques for smart grid control and management: A review," *Energies*, vol. 14, p. 1079, Feb. 2021.

[8] S. U. Ahmed, M. Affan, M. I. Raza, and M. H. Hashmi, "Inspecting mega solar plants through computer vision and drone technologies," in *Proc. Int. Conf. Frontiers Inf. Technol. (FIT)*, Islamabad, Pakistan, Dec. 2022, pp. 18–23.

[9] T. M. Adeyemi-Kayode, S. Misra, R. Maskeliunas, and R. Damasevicius, "A bibliometric review of grid parity, energy transition and electricity cost research for sustainable development," *Heliyon*, vol. 9, no. 5, May 2023, Art. no. e15532, doi: 10.1016/j.heliyon.2023.e15532.

[10] F. A. Al-Sulaiman and N. F. Al-Muthairi, "Renewable energy potential in Saudi Arabia: A comprehensive review," *Renew. Energy*, vol. 167, pp. 87–103, Oct. 2021.

[11] G. Zhang and J. Hu, "A review of short-term solar power forecasting," *Appl. Energy*, vol. 233, pp. 447–457, Jan. 2019.

[12] M. Nour, A. Labrique, and R. Labban, "Solar power forecasting: A review," *Renew. Sustain. Energy Rev.*, vol. 134, Dec. 2020, Art. no. 110321.

[13] S. Prajapati and A. Tiwari, "An empirical analysis of machine learning techniques for solar energy forecasting," *Int. J. Green Energy*, vol. 18, pp. 1217–1232, Mar. 2021.

[14] M. Abubakar, Y. Che, L. Ivascu, F. M. Almasoudi, and I. Jamil, "Performance analysis of energy production of large-scale solar plants based on artificial intelligence (machine learning) technique," *Processes*, vol. 10, no. 9, p. 1843, Sep. 2022.

[15] H. Zou, Y. Zhang, X. Li, L. Wang, and X. Chen, "Short-term power forecasting of photovoltaic power plants using a hybrid model of ARIMA and LSTM," *Appl. Energy*, vol. 288, Apr. 2021, Art. no. 116545.

[16] R. Maskeliūnas, R. Pomarnacki, V. K. Huynh, R. Damaševičius, and D. Plonis, "Power line monitoring through data integrity analysis with Q-learning based data analysis network," *Remote Sens.*, vol. 15, no. 1, p. 194, Dec. 2022, doi: 10.3390/rs15010194.

[17] G. Gupta, A. K. Singh, and A. Pandey, "Electricity generation forecasting of solar PV plant using Bi-LSTM model," *Energy Rep.*, vol. 7, pp. 303–309, Nov. 2021.

[18] M. A. Boudia, A. Mohamed, B. Haddou, and M. E. H. Benbouzid, "Short-term prediction of PV power output using hybrid ARIMA and LSTM model," *IEEE Access*, vol. 8, pp. 192526–192534, 2020.

[19] W. Gao, J. Xu, J. Yang, W. Wu, and H. Liu, "Comparison of ARIMA, LSTM, and ELM models for short-term wind power forecasting," *J. Cleaner Prod.*, vol. 318, Oct. 2022, Art. no. 128421.

[20] M. Zheng, Y. Liu, Y. Zhang, and L. Chen, "A comparative study of ARIMA, LSTM, and random forest models for wind power forecasting," *Energy Rep.*, vol. 7, pp. 2314–2324, Nov. 2021.

[21] X. Chen, Y. Ren, and Y. Wang, "Comparison of ARIMA, LSTM, and SVR models for electricity demand forecasting," *IEEE Access*, vol. 9, pp. 146172–146180, 2021.

[22] F. Khorshidian, M. Parvania, and M. Fotuhi-Firuzabad, "Comparison of ARIMA, LSTM, and MLP models for solar power forecasting," *Energy Convers. Manag.*, vol. 242, Aug. 2021, Art. no. 114231.

[23] S. Wang, M. Guo, Z. Li, and W. Zheng, "Short-term electricity demand forecasting: A comparative study of ARIMA, LSTM, and LSTM-ATT models," *Complexity*, vol. 2021, May 2021, Art. no. 6629865.

[24] S. N. Makhadmeh, M. A. Al-Betar, Z. A. A. Alyasseri, A. K. Abasi, A. T. Khader, R. Damaševičius, M. A. Mohammed, and K. H. Abdulkareem, "Smart home battery for the multi-objective power scheduling problem in a smart home using grey wolf optimizer," *Electronics*, vol. 10, no. 4, p. 447, Feb. 2021, doi: 10.3390/electronics10040447.

[25] D. Machalek, J. Tuttle, K. Andersson, and K. M. Powell, "Dynamic energy system modeling using hybrid physics-based and machine learning encoder–decoder models," *Energy AI*, vol. 9, Aug. 2022, Art. no. 100172.

[26] B. P. Mukhoty, V. Maurya, and S. K. Shukla, "Sequence to sequence deep learning models for solar irradiation forecasting," in *Proc. IEEE Milan PowerTech*, Milan, Italy, Jun. 2019, pp. 1–6, doi: 10.1109/PTC.2019.8810645.

[27] Y. Zhang, C. Qin, A. K. Srivastava, C. Jin, and R. K. Sharma, "Data-driven day-ahead PV estimation using autoencoder-LSTM and persistence model," *IEEE Trans. Ind. Appl.*, vol. 56, no. 6, pp. 7185–7192, Nov. 2020.

[28] Y. Q. Neo, T. T. Teo, W. L. Woo, T. Logenthiran, and A. Sharma, "Forecasting of photovoltaic power using deep belief network," in *Proc. IEEE Region 10 Conf. (TENCON)*, Nov. 2017, pp. 1189–1194.

[29] L.-L. Li, P. Cheng, H.-C. Lin, and H. Dong, "Short-term output power forecasting of photovoltaic systems based on the deep belief net," *Adv. Mech. Eng.*, vol. 9, no. 9, pp. 1–3, 2017.

[30] A. Gensler, J. Henze, B. Sick, and N. Raabe, "Deep learning for solar power forecasting—An approach using autoencoder and LSTM neural networks," in *Proc. IEEE Int. Conf. Syst., Man, Cybern. (SMC)*, Oct. 2016, pp. 2858–2865.

[31] M. Abdel-Nasser and K. Mahmoud, "Accurate photovoltaic power forecasting models using deep LSTM-RNN," *Neural Comput. Appl.*, vol. 31, no. 7, pp. 2727–2740, Oct. 2017.

[32] Y. Chen, M. S. Bhutta, M. Abubakar, D. Xiao, F. M. Almasoudi, H. Naeem, and M. Faheem, "Evaluation of machine learning models for smart grid parameters: Performance analysis of ARIMA and Bi-LSTM," *Sustainability*, vol. 15, no. 11, p. 8555, May 2023.

[33] W. Wei, H. Wu, and H. Ma, "An autoencoder and LSTM-based traffic flow prediction method," *Sensors*, vol. 19, no. 13, p. 2946, Jul. 2019, doi: 10.3390/s19132946.

AHSAN ZAFAR was born in Peshawar, Pakistan. He received the B.S. degree in electrical engineering from the University of Engineering and Technology, Peshawar, in 2015, and the M.S. degree in electrical engineering from COMSATS University, Islamabad, in 2019. He is currently pursuing the Ph.D. degree with the School of Electrical and Information Engineering, Tianjin University, China. His current research interests include the forecasting power generation in smart grids via machine learning and deep learning models.

YANBO CHE (Member, IEEE) was born in Shandong, China. He received the B.S. degree from Zhejiang University, Hangzhou, China, in 1993, and the M.S. and Ph.D. degrees from Tianjin University, Tianjin, China, in 1996 and 2002, respectively, all in electrical engineering. Since 1996, he has been engaged in teaching and scientific research of power electronic technology and power systems. He is currently a Professor with the School of Electrical and Information Engineering, Tianjin University. His current research interests include power systems, renewable energy resources, and microgrids.

MUNEER AHMED received the B.Eng. degree from QUEST University, Pakistan, and the M.S. degree in electrical and computer engineering from the South China University of Technology, Guangzhou, China, in 2021. He is currently pursuing the Ph.D. degree with the School of Electrical Engineering, Tianjin University, China. He was a Lead Engineer with Tianjin Jinsheng Jida New Energy Company Ltd., for two years. His current research interest includes machine learning models approach in micro grids.

MUHAMMAD SARFRAZ received the B.Eng. degree from the Sukkur Institute of Business Administration University, Pakistan, and the M.S. degree from North China Electric Power University, Beijing, in 2020. He is currently pursuing the Ph.D. degree with the School of Electrical and Information Engineering, Tianjin University, China. His current research interests include battery life cycle monitoring and battery management system using machine learning models.

ASHFAQ AHMAD received the master's degree in chemistry from the University of Malakand, Khyber Pakhtunkhwa, Pakistan, in 2005, and the Ph.D. degree in analytical chemistry from King Saud University, Saudi Arabia. He is currently an Assistant Professor with the Chemistry Department, College of Science, King Saud University. His current research interests include materials synthesis and activation of carbonaceous materials from biomass waste and their environmental applications in adsorption of metals, ions, and dyes.

MOHAMMAD ALIBAKHSHIKENARI (Member, IEEE) was born in Mazandaran, Iran, in February 1988. He received the Ph.D. degree (Hons.) (European Label) in electronics engineering from the University of Rome "Tor Vergata," Italy, in February 2020. From May 2018 to December 2018, he was a Ph.D. Visiting Researcher with the Chalmers University of Technology, Gothenburg, Sweden. His training during the Ph.D. research visit included a research stage with Swedish Company Gapwaves AB, Gothenburg. Since July 2021, he has been with the Department of Signal Theory and Communications, Universidad Carlos III de Madrid (uc3m), Spain, as a Principal Investigator of CONnecting EXcellence (CONEX)-Plus Talent Training Program and Marie Skłodowska-Curie actions. He was a Lecturer of electromagnetic fields and electromagnetic laboratory with the Department of Signal Theory and Communications, for the academic year 2021–2022. From December 2022 to May 2023, he spent three industrial and academic research visits with SARAS Technology Company Ltd., Leeds, England, U.K.; Edinburgh Napier University, Edinburgh, Scotland, U.K.; and the University of Bradford, West Yorkshire, England, which were defined by CONEX-Plus Talent Training Program and Marie Skłodowska-Curie Actions as his secondment research visit plans. His research interests include electromagnetic systems, antennas and wave-propagations, metamaterials and metasurfaces, sensors, synthetic aperture radars (SAR), 5G and beyond wireless communications, multiple input multiple output (MIMO) systems, RFID tag antennas, substrate integrated waveguides (SIWs), impedance matching circuits, microwave components, millimeter-waves and terahertz integrated circuits, gap waveguide technology, beamforming matrix, and reconfigurable intelligent surfaces (RIS), which led to achieve more than 4700 citations and H-index above 43 reported by Scopus, Google Scholar, and ResearchGate. He was a recipient of the three years Principal Investigator Research Grant funded by Universidad Carlos III de Madrid and the European Union's Horizon 2020 Research and Innovation Program under the Marie Skłodowska-Curie Grant started in July 2021; the two years Postdoctoral Research Grant funded by the University of Rome "Tor Vergata" started in November 2019; the three years Ph.D. Scholarship funded by the University of Rome "Tor Vergata" started in November 2016; and the two Young Engineer Awards of the 47th European Microwave Conference, held in Nuremberg, Germany, in 2017, and the 48th European Microwave Conference, held in Madrid, Spain, in 2018. In April 2020, his research article entitled "High-Gain Metasurface in Polyimide On-Chip Antenna Based on CRLH-TL for Sub Terahertz Integrated Circuits" published in Scientific Reports was awarded as the Best Month Paper at the University of Bradford, West Yorkshire, England. He also received the "Teaching Excellent Acknowledgement" Certificate for the course of electromagnetic fields from the Vice-Rector of studies of uc3m. He acts as a referee in several highly reputed journals and international conferences. He is serving as an Associate Editor for *Radio Science* and *IET Journal of Engineering*.